CRYSTAL GROWTH & DESIGN

Article

pubs.acs.org/crystal

Syntheses, Crystal Structures, and Properties of Two 2-Fold Interpenetrating Metal–Organic Frameworks Based on a Trigonal Rigid Ligand

Jie Yang,[†] Xiaoqing Wang,[†] Rongming Wang,[‡] Liangliang Zhang,*[,‡] Fuling Liu,[†] Fangna Dai,[‡] and Daofeng Sun*[,†,‡]

[†]Key Laboratory of Colloid and Interface Chemistry, Ministry of Education, School of Chemistry and Chemical Engineering, Shandong University, Jinan, Shandong 250100, People's Republic of China

[‡]College of Science, China University of Petroleum (East China), Qingdao, Shandong 266580, People's Republic of China

Supporting Information

ABSTRACT: Two 2-fold interpenetrating metal–organic frameworks based on 1,3,5-tris[2-(4-carboxyphenyl)-1-ethynyl]-2,4,6-trimethylbenzene (H_3L^{Me}), $[Mn_3(L^{Me})_2(DMF)_4(H_2O)]\cdot 1.5DMF\cdot 3.5H_2O$ (**1**) and $[Cd_3(L^{Me})_2(DMF)][Cd_3(L^{Me})_2(DMF)_2(H_2O)]\cdot 5DMF\cdot 3.5H_2O$ (**2**), have been synthesized by using rigid trigonal H_3L^{Me} and nitrate under solvothermal conditions. Complex **1** displays a three-dimensional open framework with rare (3,6)-connected 2-nodal ***sit*** topology, whereas complex **2** features a new (3,3,6)-connected topology. Both **1** and **2** are blue fluorescent, and the magnetic measurement of **1** indicates that metal centers within the trinuclear cluster exhibit antiferromagnetic coupling interactions. Significantly, although complexes **1** and **2** have similar total solvent-accessible volumes, **2** demonstrates a higher Brunauer–Emmett–Teller surface area than that of **1**, further indicating the influence of pore structure on gas absorption.

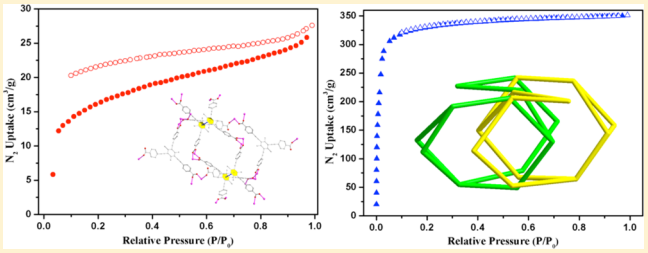

INTRODUCTION

Metal–organic frameworks (MOFs) have become a hot research interest in the porous materials field, due to their incomparable characteristics in structural variety as well as their fundamental and industrial contributions.[1−3] The self-assembly characteristic of the covalent bonds between metal clusters and organic linkers results in MOFs turning into ordered crystalline materials with high Brunauer–Emmett–Teller (BET) surface area, which makes them useful for various applications in areas including gas storage,[4,5] luminescence,[6−10] catalysis,[11−14] separation,[15−17] chirality,[18,19] biotechnology,[20−22] magnetism,[23−27] and so forth. Thus, constructing the desired nature and structure of MOFs is one of the rapidly growing research areas in the chemical field over the last few decades.

A number of basics might influence the structures and properties of MOF materials, such as the various metal centers, organic linkers, and subsidiary molecules.[28,29] As is well-known, the organic ligand plays a key part in self-assembly and determination of the configurable and functional nature of the MOFs. In general, the distance from the linker core to each pair of carboxylates increases when lengthening organic ligands, and thus the MOF pore size also enlarges, for instance, MOF-5, HKUST-1, MOF-177, MOF-399, MOF-14, PCN-6, MOF-143, and MOF-388.[30−33] Moreover, Mn^{2+}, Mn^{3+}, Ni^{2+}, Co^{2+} ions provide variations of magnetic anisotropy and spin quantum number due to their unpaired electrons per ion; and the d^{10} metals are excellent candidates in the construction of luminescent molecular materials.[34−37] These different characteristics enable us to produce luminescent and magnetic MOF materials which are crucial to lighting, optical equipment, thin film, and magnetic memory materials.[38] Consequently, designing new organic ligands and assembling with suitable metal ions are still an important research subject.

Among the carboxylate ligands, trigonal carboxylate ligands based on C_3 symmetry have become the focus of attention due to the structure multiformity in constructing porous materials, such as 4,4′,4″-(benzene-1,3,5-triyl-tris(ethyne-2,1-diyl))-tribenzoate (H_3BTE), 4,4′,4″-(2,4,6-trimethylbenzene-1,3,5-triyl)tribenzoic acid (H_3TMTA), and 4,4′,4″-benzene-1,3,5-triyltribenzoate (H_3BTB).[39,40] These ligands can easily form C_3-symmetric tricarboxylate linkers and construct MOF materials with high surface area. Bearing all of this in mind, we prepared a new trigonal carboxylate ligand, 1,3,5-tris[2-(4-carboxyphenyl)-1-ethynyl]-2,4,6-trimethylbenzene (H_3L^{Me}), which has not been reported yet. Its triangular nodal topology is characterized by a carboxylate–carboxylate and centroid–carboxylate separation distance of calc. 17 Å and 10 Å, respectively. H_3L^{Me} was selected due to the following factors: (i) the characteristic of the organic ligand may promote the formation of novel network topologies; (ii) it can exhibit a

Received: September 23, 2014
Revised: November 12, 2014
Published: November 13, 2014

   dx.doi.org/10.1021/cg501425x | *Cryst. Growth Des.* 2014, 14, 6521−6527

variety of coordination modes through the carboxylate oxygen atom; (iii) H_3L^{Me} ligand and metal ions via coordination bonds may generate multinuclear and high-dimensional self-penetrating or interpenetrating nets. In this work, through the self-assembly of H_3L^{Me} with manganese and cadmium salts, two porous metal−organic frameworks are obtained. Single crystal diffraction analysis data display that both MOFs possess three-dimensional (3D) honeycomb 2-fold interpenetrating frameworks based on a trinuclear $[M_3(COO)_6]$ secondary building unit (SBU) and Y-shaped trinodal organic linker. The magnetic measurement of complex **1** indicates that antiferromagnetic interactions exist between the manganese ions. Photoluminescent investigation shows that complex **2** possesses a strong luminescent property when compared to complex **1** due to the cadmium ion. Although two complexes have similar solvent-accessible volumes, complex **2** possesses a higher BET surface area than that of **1**.

EXPERIMENTAL SECTION

All chemical analytical grade reagents employed were used as commercially. H_3L^{Me} was synthesized using a Sonogashira coupling approach (Scheme 1). Powder X-ray diffraction (PXRD) pattern

Scheme 1. Synthetic Procedures of H_3L^{Me}

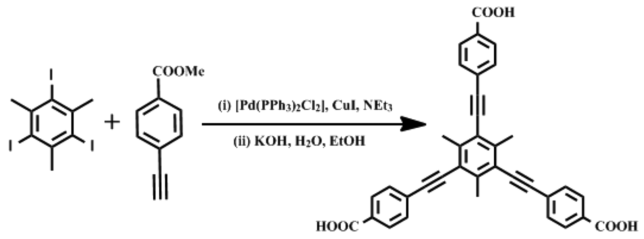

experiments were carried on a Bruker AXS D8 instrument. The IR spectra were operated on a Nicolet 330 FTIR spectrometer. Thermogravimetric experiments (TGA) were performed using a PerkinElmer TGA7 instrument. The data of luminescence spectra were recorded using an F-280 fluorescence spectrophotometer. The measurements of elemental analysis were using a PerkinElmer 240 elemental instrument. The magnetic property was analyzed using a Squid-VSM, Quantum Design. The measurements of gas uptake were performed using a Micrometritics ASAP 2020 instrument at various gases and temperatures.

Synthesis of Complex 1 $[Mn_3(L^{Me})_2(DMF)_4(H_2O)]\cdot 1.5DMF\cdot 3.5H_2O$ (1). $MnCl_2\cdot 4H_2O$ (3.0 mg, 0.015 mmol) and H_3L^{Me} (1.1 mg, 0.0020 mmol) were dissolved in DMF (1.0 mL) and then sealed and heated to 90 °C for 48 h. The reaction was cooled to room temperature in 800 min. Light yellow flaky crystals of **1** were obtained and dried at system temperature (yield: 50%, based on manganese). Elemental analysis calcd (%) for **1**: $C_{89.5}H_{91.5}O_{23}N_{5.5}Mn_3$: C, 60.49; H, 5.19; N, 4.37. Found: C, 60.13; H, 5.07; N, 4.45. IR data (KBr cm^{-1}): 3430(w), 2926(w), 1655(s), 1602(m), 1538(s), 1389(m), 1098(w), 863(w), 783(w), 700(s), 576(w), 419(w).

Synthesis of Complex 2 $[Cd_3(L^{Me})_2(DMF)_3][Cd_3(L^{Me})_2(DMF)_2(H_2O)]\cdot 5DMF\cdot 3.5H_2O$ (2). A mixture of $Cd(NO_3)_2\cdot 4H_2O$ (3.1 mg, 0.010 mmol), H_3L^{Me} (1.1 mg, 0.0020 mmol), 1.0 mL of DMF was placed in a sealed glass tube. The final mixture was sealed in a glass vial and heated at 120 °C for 48 h. Yellow needle crystals of **2** were gained and dried at indoor temperature (yield: 40%, based on cadmium). Elemental analysis calcd (%) for **2**: $C_{174}H_{164}O_{38.5}N_{10}Cd_6$: C, 56.7; H, 4.49; N, 3.80. Found: C, 57.03; H, 4.21; N, 3.68. IR data (KBr cm^{-1}): 3423(w), 2925(w), 2201(w), 1651(s), 1580(m), 1532(m), 1385(s), 125(w), 1095(m), 858(m), 780(s), 699(w), 665(w), 526(w), 416(w).

X-ray Structural Crystallography. The data of two crystals were measured on an Agilent Super nova and a Bruker APEXII CCD diffractometer with Mo−Kα radiation source (λ = 0.71073 Å), respectively. The absorption corrections of two crystals were employed by the program *SADABS*.[41] Structures were refined with anisotropy on F^2, and by full-matrix least-squares with *SHELXTL*-97.[42] The *SQUEEZE* procedure was applied to eliminate the disordered solvent molecules, and then a new file was generated. Two crystal structures were inspected through the Addsym subprogram of *PLATON*[43] to determine that no attached symmetry should be used for the models. Two crystallographic data are presented in Table 1, and the sectional bond lengths and angles are presented in Tables S1 and S2. The topological analyses and some graphs were generated applying the TOPOS program.[44] CCDC numbers (1009434, 1009435) include the supplementary crystallographic data, which have been come from the Cambridge Crystallographic Data Center.

Table 1. Crystallographic Data for Complexes 1 and 2

	1	2
empirical formula	$C_{84}H_{72}O_{17}Mn_3N_4$	$C_{159}H_{122}O_{30}Cd_6N_5$
formula weight	1574.28	3257.02
temperature (K)	150.00(10)	273.15
crystal system	triclinic	orthorhombic
space group	$P\bar{1}$	$Pna2_1$
a (Å)	13.8783(5)	42.439(10)
b (Å)	20.3674(8)	13.969(4)
c (Å)	21.0344(5)	33.470(8)
α (deg)	62.572(3)	90.00
β (deg)	82.489(3)	90.00
γ (deg)	73.850(3)	90.00
volume (Å^3)	5069.1(3)	19842(9)
Z	2	4
ρcalc (g/cm^3)	1.031	1.090
μ (mm^{-1})	0.422	0.687
F (000)	1630.0	6556.0
data/restraints/params	18916/4/987	33438/1/1823
GOF on F^2	1.004	1.007
final R indices $[I > 2\sigma(I)]^a$	R_1 = 0.1153	R_1 = 0.0866
	wR_2 = 0.3542	wR_2 = 0.1842

$^aR_1 = \sum||F_o| - |F_c||/|\sum o|$. $wR_2 = \{\sum[w(F_o^2 - F_c^2)^2]/\sum[w(F_o^2)^2]\}^{1/2}$.

RESULTS AND DISCUSSION

Synthesis and Characterization. 1,3,5-Tris[2-(4-carbomethoxyphenyl)-1-ethynyl]-2,4,6-trimethylbenzene was synthesized using Sonogashira coupling of 1,3,5-triiodo-2,4,6-trimethylbenzene with methyl 4-ethynylbenzoate, and then H_3L^{Me} was obtained through hydrolysis reaction. The course was displayed in Scheme 1, and the synthetic details were shown in Supporting Information.

Crystal Structure. The crystal structure reveals that **1** crystallizes in triclinic space group $P\bar{1}$ and possesses a 3D honeycomb framework based on trinuclear SBUs and C_3-symmetric ligands with a ***sit*** topology. Figure 1a exhibits that the asymmetric unit includes three equivalent Mn(II) ions, two $(L^{Me})^{3-}$ ligands, one coordinated water molecule, and four coordinated DMF molecules. Mn1 is six coordinated, connected by three O atoms from three $(L^{Me})^{3-}$ ligands, O1, O2 from DMF molecules and O1w from water molecule, demonstrating a distorted octahedral geometry. Mn2 is surrounded by six O atoms from four different $(L^{Me})^{3-}$ ligands. Mn3 is also six coordination, located in tiny distorted octahedral configurations, connected by two O from DMF molecules and the other coordinated O from four $(L^{Me})^{3-}$ ligands. The Mn−O covalent bond distances are within the range of 2.096 (4)−2.360 (4) Å, which is consistent with the

dx.doi.org/10.1021/cg501425x | Cryst. Growth Des. 2014, 14, 6521−6527

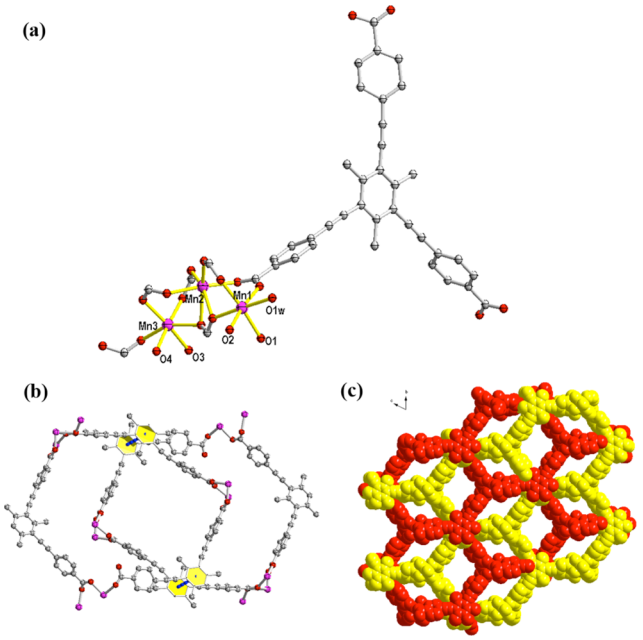

Figure 1. (a) Coordination mode of metal ions for complex **1**. (b) The $\pi\cdots\pi$ stacking between two $(L^{Me})^{3-}$ ligands in different nets. (c) 3D porous 2-fold interpenetrating framework viewed from the *a* axis direction.

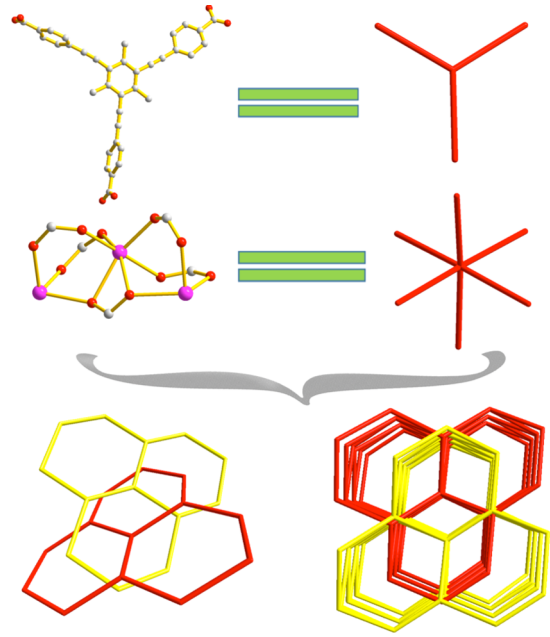

Figure 2. A graphical representation of a simplified 2-fold interpenetrating porous 3D framework for **1** with ***sit*** topology containing two types of nodes.

other reported manganese complexes.[45−49] The $(L^{Me})^{3-}$ ligands possess two coordination modes: μ^5-η^2:η^0:η^1:η^1:η^1 and μ^7-η^2:η^1:η^1:η^1:η^1:$\eta^1\eta^1$ (a, b in Scheme S1). As illustrated in Figure 1b, a hexagonal plane is formed by three trinuclear SBUs and three carboxylate benzene groups, where three trinuclear SBUs act as the three points of the hexagonal, and the other vertices and edges are combined by $(L^{Me})^{3-}$ ligands to generate hexagonal enterclose. The whole framework is further formed by the $\pi\cdots\pi$ stacking between the aromatic ring center of the near carboxylic acid and another aromatic ring center of $(L^{Me})^{3-}$ ligand in the other framework (the centroid−centroid distance is 3.6 Å). The observed interpenetration mode is highlighted in Figure 1b. Each Y-shape $(L^{Me})^{3-}$ ligand connects three trinuclear SBUs, the trinuclear Mn cluster and the rigid trigonal carboxylate ligand were generated a two-dimensional (2D) framework. The $\pi\cdots\pi$ stacking between the two single net further stabilize the interpenetration, and it reveals a 3D 2-fold interpenetrating network with one-dimensional (1D) channels along the *a* axis (Figure 1c). The dimensions of the channels in the single net are approximately 18.76 Å × 17.51 Å along the *a* axis, and after interpenetration, the dimensions changed to 14.51 Å × 8.51 Å, in which uncoordinated DMF and water molecules are taken up. The total volume is 23.5% for **1**, as obtained by PLATON routine.

To fully comprehend this crystal structure of complex **1**, we have used the TOPOS software to execute topological analysis of the porous 3D framework.[50] The topological structure displayed a 2-nodal (3, 6)-connected network, and its stoichiometry is (3-c)2(6-c), in which each Mn_3−SBU is taken as a 6-coordinated node and each $(L^{Me})^{3-}$ ligand as a 3-coordinated node. It is interesting to note that the 3-connected and 6-connected relationship is 2 to 1, illustrating that this 3D framework is a 2-fold interpenetrating structure with rare ***sit*** topology[51] (Figure 2). The Schäfli notation is $\{4.6^2\}_2\{4^2.6^{10}.8^3\}$ and the complicated symbol is [4.4.6.6.6.6.6.6.6.6.6(2).6(2).-8.8.8(6)] [4.6(2).6(2)].

The datum analysis of crystal indicates that **2** crystallizes in orthorhombic *Pna*21 space group. It is interesting that the asymmetric unit is composed of two individual networks founded on a similar SBU. The asymmetric unit of both networks consists of two ligands, three cadmium ions, and three coordinated solvate molecules. Both networks are based on a trinuclear SBU, and the only difference between these two networks is the coordinated solvates on Cd ions: Cd3 and Cd4, on which one is coordinated by three DMF molecules and the other is by two DMF and one water molecules. In these two SBUs, five Cd (II) atoms are all in a six-coordinated mode, showing octahedral geometry; only Cd6 exhibits a tetragonal pyramidal coordination conformation via five covalent bonds. The details of the above description as displayed in Figure 1a. In this reaction, all carboxylic acid groups from the H_3L^{Me} were generated by the reaction of deprotonation via the assembly process. The $(L^{Me})^{3-}$ ligands possess three types of coordination modes: μ^7-η^2:η^1:η^1:η^1:η^1:η^1:η^1, μ^5-η^2:η^1:η^1:η^1:η^1, μ^5-η^2:η^1:η^2:η^1:η^1 (b−d in Scheme S1). The Cd−O covalent bond lengths are within the range of 2.094(10)−2.562(8) Å, which is consistent with the other reported cadmium complexes.[52] As shown in Figure 3b, the two SBUs were connected by the backbones of the $(L^{Me})^{3-}$ ligands to generate two independent open frameworks with 1D channels along the *b* axis. The dimensions of the channels are 21.21 Å × 18.14 Å. These two independent frameworks interpenetrate each other through strong $\pi\cdots\pi$ interaction (3.525 Å) between two central benzene rings of the organic ligands in different nets. After the interpenetration, the dimensions of the channels changed to 12.83 Å × 11.99 Å.

To achieve insight into the 3D network, topological analysis for **2** was implemented via the corresponding software. The picturesque and attractive structural characteristic of **2** is that this 3D porous framework can be reasonable simplified to a unique 3-nodal net with an unprecedented $\{4.6.8\}_2$-$\{4^2.6^5.8^6.10^2\}$ topology. Interestingly, the asymmetric unit includes two individual networks based on a similar SBU.

dx.doi.org/10.1021/cg501425x | *Cryst. Growth Des.* 2014, 14, 6521−6527

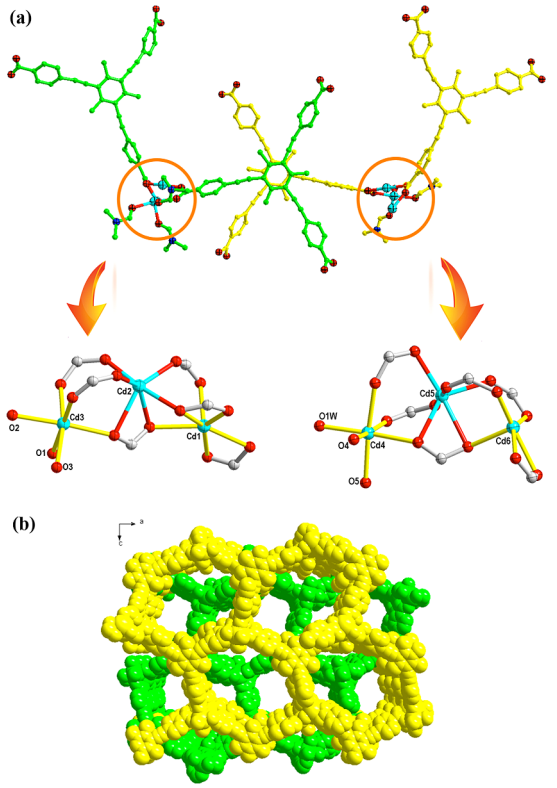

Figure 3. (a) Coordination mode of metal ions for complex **2**. (b) 3D porous 2-fold interpenetrating framework viewed from the *b* axis direction.

Through the analysis of TOPOS software, each of two $(L^{Me})^{3-}$ ligands is simplified as 3-connected nodes due to its different coordinated configuration with the point symbol of {4.6.8}, respectively. Therefore, the stoichiometry is (3-c)(3-c), and two Cd-SBUs can be regarded as 6-connected node with the point symbol of $\{4^2.6^5.8^6.10^2\}$. Thus, two independent units via strong $\pi\cdots\pi$ interactions form a 2-fold interpenetrating 3D network, which is a 3-nodal (3,3,6)-connected network (Figure 4).[53] A few reports of a similar topological structure, such as (3,6)-, (3,6,6)-connected nets,[54,55] were acquired by consulting various literature reports. However, within the scope of our knowledge, no reports of these types of (3,3,6)-connected 3-nodal or interpenetrating modal structures have been named in the topology database.

Analyses of Powder Diffraction, IR Spectra, Thermogravimetry and Luminescent Properties. The two complexes were acquired under different temperatures in a sealed glass tube through a solvothermal reaction, synthesized by using rigid trigonal H_3L^{Me} and nitrate.[56] The data of powder diffraction and IR spectrum for complexes **1** and **2** have been measured to establish the purities and structures, which are revealed in Figures S1 and S2, Supporting Information, respectively.

The thermogravimetric analysis (TGA) experiments of samples **1** and **2** were measured in a N_2 ambience with a heating range of 25−800 °C. The TGA curves of two samples are presented in Supporting Information S3. The TGA chart of sample **1** displays a weight loss of 4.7% (calculated 4.6%) in the 25−69 °C range ascribed to the loss of lattice water; whereafter, another 23.0% weight loss from 70 to 322 °C (calculated 23.6%) is in accordance with the elimination of five and a half DMF molecules and one coordinated water molecule;

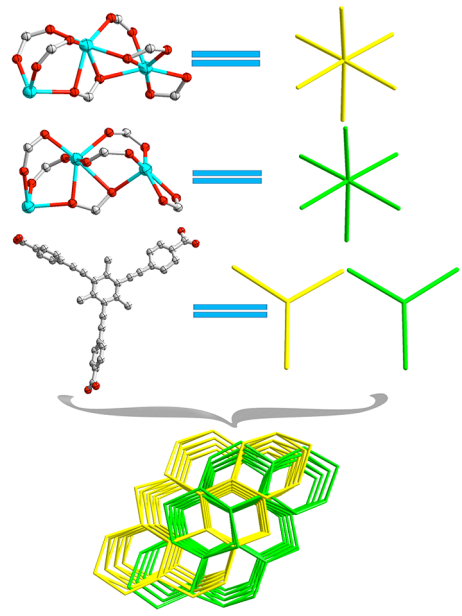

Figure 4. A graphical representation of a simplified 2-fold interpenetrating porous 3D network for **2** with 3,3,6-c topology containing three types of nodes.

subsequently, the framework starts to decompose. The curves of **2** exhibiting a weight loss of 22.1% is equivalent of the loss of four and a half water molecules and 10 DMF molecules from 25 to 244 °C (calculated 22.0%); upon further heating, the organic framework collapses to form oxide components.

The luminescent properties of MOFs are interesting because of their various applications in biomedicine, light-emitting devices and chemical sensors, and the like.[57−59] General d^{10} transition metal are remarkable candidates in the construction of photoluminescence materials because the metal is hard to oxidize or reduce.[60−64] Meanwhile, the coordination modes of organic ligands and different metals also affect the emission wavelength and luminescent theory.[65] The luminescent properties of H_3L^{Me} and complexes **1** and **2** were tested in the solid state at room temperature (clear data as revealed in Figure 5). The photoluminescence datum of free H_3L^{Me} ligand displays an emission maxima peak at 440 nm (λ_{ex} = 300 nm), which is ascribed to the $\pi^* \rightarrow$ n or $\pi^* \rightarrow \pi$ transitions.[66−68] The

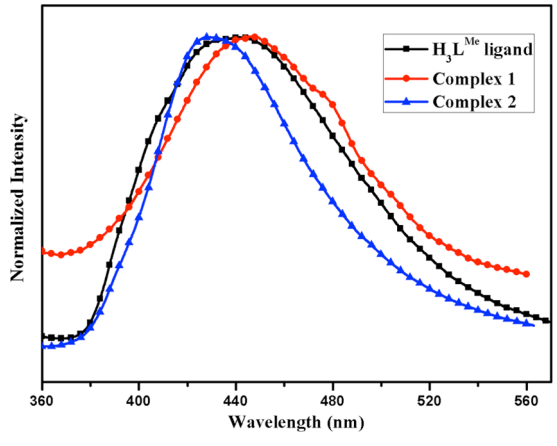

Figure 5. Photoluminescences of H_3L^{Me} ligand and complexes **1** and **2**.

dx.doi.org/10.1021/cg501425x | *Cryst. Growth Des.* 2014, 14, 6521−6527

maxima peaks of two MOFs are at 448 nm (λ_{ex} = 295 nm) and 428 nm (λ_{ex} = 300 nm), respectively. The maxima peak of **1** is red-shifted by 8 nm, and a blue shift of 12 nm has been presented in **2** in contrast to those of the free H_3L^{Me} ligand. The difference phenomenon shows that the electronic configuration characteristics of Mn and Cd are different; the latter one is difficult to oxidize or reduce.[69] Furthermore, different coordination environments of central metal ions resulting in the ligand $\pi^*\cdots\pi$ transitions is also another factor.

Magnetic Properties for Complex 1. Because complex **1** includes three Mn^{II} ions, the measurement of magnetic properties was performed under a 1000 Oe applied field. The details of the $\chi_M T$ versus T plot at the temperature ranging from 1.8 to 300 K are exhibited in Figure 6a, of which χ_M is the

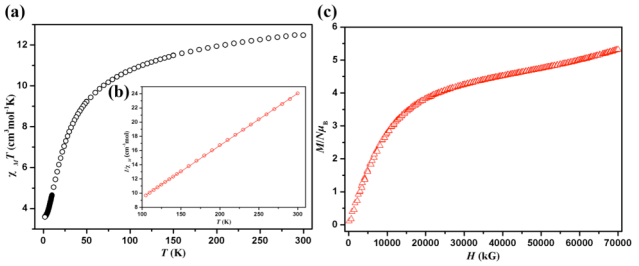

Figure 6. (a) The magnetic susceptibility curve of $\chi_M T$ versus T. (b) The $1/\chi_M$ versus T plots is the Curie–Weiss fitting. (c) M–H curve in the 1–7 T magnetic filed ranges.

explanation of greater susceptibility of each Mn^{II}_3 unit. Complex **1** exhibits a dominant antiferromagnetic exchange between the Mn^{II} ions. The values of $\chi_M T$ continually decrease as the temperature decreases and descend sharply after 75 K. The $\chi_M T$ value reaches the maximum at 300 K of 12.5 cm^3 mol^{-1} K, which is slightly lower than the calculation of the theoretical value (13.125 cm^3 mol^{-1} K) with the presence of three uncoupled Mn^{II} ions. Generally, in most of Mn^{II} complexes, assuming g = 2.0, the magnetic torque at 300 K is slightly lower than the calculative value, that is to say, the Lande factor of Mn^{II} is lower than 2.0. Furthermore, the antiferromagnetic coupling effect among manganese ions could likewise cause a lower value than those of a corresponding theoretical one. The magnetic susceptibility abides by the formula $\chi = C/(T - \theta)$ below 100 K, which is named the Curie–Weiss law, and it is further supported by a well-fitted χ_M^{-1} versus T plot that gives C (Curie constant) = 13.63 cm^3 mol^{-1} K and θ (Weiss constant) = −27.91 K (Figure 6b). The measurement of DC magnetization was performed at 1.8 K in the 1–7 T magnetic field ranges. The magnetization increases in all the fields. The field dependence of magnetization quickly increases to 3.86 μ_B at the point of 2 T and finally reaches a saturation state. The magnetization value of 5.3 μ_B at the point of 7 T is much lower than that of M_{Mn3} with the theoretical saturation value of 15 μ_B, indicating not a strong enough field to cause the spins of $[Mn_3]$ to arrange in parallel entirely along the direction of the applied field. The magnetization curve manifests that complex **1** has antiferromagnetic interaction (Figure 6c). In order to research the dynamics of the effect of magnetization relaxation, the *ac* magnetic susceptibility was measured under a 5.0 Oe *ac* field adding a zero applied *dc* field in the 1.8–20 K temperature ranges and in the 1–500 Hz frequency range. The diagram of in-phase and out-of-phase *ac* magnetic susceptibility versus T is displayed in Supporting Information S4. The graph was generated without magnetic frequency-dependence, and the complex **1** does not exhibit three-dimensional *ac* signals.

Gas Adsorption Analyses. The measurement of adsorption properties of complexes **1** and **2** have been performed on a Micrometritics ASAP 2020 system. Two MOFs were sequentially exchanged with methanol and dichloromethane, and the degassing process was performed at 40 °C for 5 h. The gas sorption capabilities of two complexes were investigated using several gases (N_2, H_2, Ar, and CO_2) at varying temperatures. The pore volumes of complexes **1** and **2** were calculated by the *PLATON*[43] program. The values are 5069.1 and 19842 $Å^3$, which corresponds with 23.5 and 30.8% of their respective unit.

The N_2 and Ar gas uptake isotherms of **1** show the type IV adsorption isotherm under 77 K temperature (Figure 7a). The

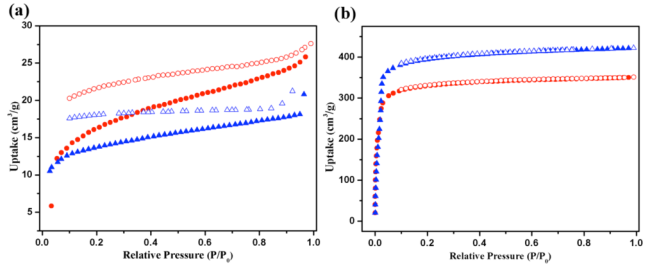

Figure 7. (a) The N_2 and Ar sorption isotherms at 77 K for complex **1**. (b) The N_2 and Ar sorption isotherms at 77 K for complex **2**. N_2: red symbols, Ar: blue symbols.

uptakes of N_2 and Ar are only 27.6 cm^3 g^{-1} and 20.8 cm^3 g^{-1} at 1 bar, respectively. The BET surface area is estimated 59.4 m^2 g^{-1} from the data of the measurement. The achieved pore volume is 0.04 $cm^3 g^{-1}$, which is much smaller than that calculated (0.23 $cm^3 \cdot g^{-1}$) from the single crystal data. This phenomenon may be interpreted as the adaptability of the weak $\pi\cdots\pi$ stacking under the high pressure, which results in the dislocation of the organic frameworks, and it is the same as other reported soft porous MOFs.[70] The desolvated complex **2** exhibits typical type-I gas uptake isotherms, indicating the presence of microporous structures after eliminating the solvent molecules (Figure 7b). The adsorption isotherms of N_2 and Ar have an abrupt slope from 0.01 to 0.1 bar, which reveals that the total pore volume is packed with the gas in the 0.01–0.1 bar pressure of the range. Then the uptake capacity of N_2 and Ar increases slightly and reaches a platform 351.2 cm^3 g^{-1} and 421.9 cm^3 g^{-1} at 1 bar, respectively. The BET surface area and pore volume are estimated to be 1353.32 m^2 g^{-1} and 0.54 cm^3 g^{-1} by measuring data, respectively.

Although complex **2** displays a higher adsorption of N_2 and Ar corresponding to higher surface area and pore volume, H_2 and CO_2 measurements of **1** and **2** show diverse results. As is shown in Figure 8, complex **1** takes up a defined amount of hydrogen, 52.7 cm^3 g^{-1} (0.47 wt %) at 77 K, 24.9 cm^3 g^{-1} of carbon dioxide at 273 K. H_2 and CO_2 adsorption capacities of complex **2** are not influenced by its high surface area or pore volume at low pressures. The results show that complex **2** at 77 K takes up a defined amount of hydrogen 76.4 cm^3 g^{-1} (0.68 wt %), which is slightly higher than that of complex **1**. However, the uptake value of carbon dioxide is 20.5 cm^3 g^{-1} at 273 K, which is lower than that of complex **1**. Although the uptake values of nitrogen and argon of complex **2** are almost 12 times

dx.doi.org/10.1021/cg501425x | *Cryst. Growth Des.* 2014, 14, 6521–6527

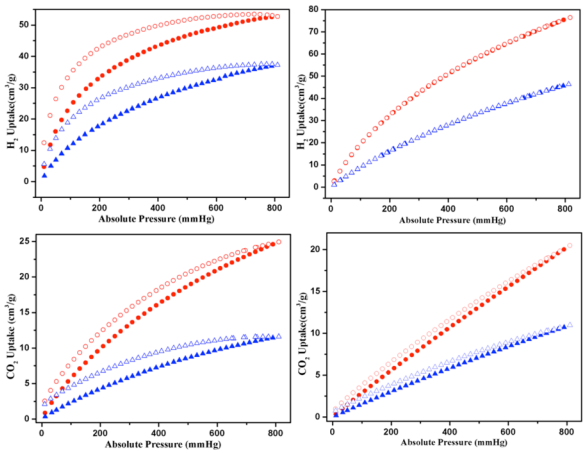

Figure 8. H_2 and CO_2 sorption isotherms for two complexes. (For complex **1**: left, complex **2**: right; H_2: red symbols, 77 K; blue symbols, 87 K; CO_2: red symbols, 273 K; blue symbols, 295 K.)

greater than that of complex **1**, the uptake capacities of H_2 and CO_2 are similar for **1** and **2**. These results further confirm that the adsorption capacity of two complexes is highly influenced by pore size and geometry.[71]

CONCLUSIONS

In summary, two 2-fold interpenetrating 3D porous MOFs based on trinuclear transition metal clusters and 1,3,5-tris[2-(4-carboxyphenyl)-1-ethynyl]-2,4,6-trimethylbenzene ligand were successfully obtained, and some basic characterization methods such as X-ray single crystal diffactometor, EA, PXRD, IR, and TGA, and so forth were carried out. Both **1** and **2** are 3D 2-fold interpenetration frameworks. Complex **1** is (3,6)-connected with rare ***sit*** topology, which interpenetrates each other through $\pi\cdots\pi$ stacking. **2** is a new (3, 3, 6)-connected network based on a trinuclear cluster and a C_3-symmetric trimethyl substituted organic linker. Fluorescence test exhibits that it produced a red shift and blue shift compared with free ligand, respectively, which is due to the different metal and coordination environments. The magnetic results reveal that the magnetic behavior of **1** should arise from the antiferromagnetic interaction among the Mn(II) ions. Gas uptake measurements on **1** and **2** reveal that complex **2** possesses a much higher surface area than that of **1**, although they exhibit similar H_2 and CO_2 uptakes, and the CO_2 uptake and Q_{st} for **1** is higher than that of **2**, further indicating the influence of pore structure on the gas absorption.

ASSOCIATED CONTENT

Supporting Information

CIF format of crystal data, preparation of H_3L^{Me} ligand, table of bond distances and angles, coordinated mode, the graphical representations of PXRD, IR spectra, and TG–DSC, heats of sorption isotherms of H_2 and CO_2 for two MOFs. This material is available free of charge via the Internet at http://pubs.acs.org.

AUTHOR INFORMATION

Corresponding Authors

*E-mail: liangliangzhang@upc.edu.cn. (L.Z.).
*E-mail: dfsun@sdu.edu.cn. (D.S.).

Notes

The authors declare no competing financial interest.

ACKNOWLEDGMENTS

This work was supported by National Natural Science Foundation of China (21271117), the Shandong Natural Science Fund for Distinguished Young Scholars (JQ201003), National Science Foundation of Shandong Province (BS2011CL041), the Fundamental Research Funds for the Central Universities (13CX05010A, 13CX02006A), and NCET-11-0309.

REFERENCES

(1) Yaghi, O. M.; O'Keeffe, M.; Ockwig, N. W.; Chae, H. K.; Eddaoudi, M.; Kim, J. *Nature* **2003**, *423*, 705–714.
(2) Ferey, G. *Chem. Soc. Rev.* **2008**, *37*, 191–214.
(3) Horike, S.; Shimomura, S.; Kitagawa, S. *Nat. Chem.* **2009**, *1*, 695–704.
(4) Ryan, P.; Farha, O. K.; Broadbelt, L. J.; Snurr, R. Q. *AIChE J.* **2011**, *57*, 1759–1766.
(5) Farha, O. K.; Yazaydin, A. O.; Eryazici, I.; Malliakas, C.; Hauser, B.; Kanatzidis, M. G.; Nguyen, S. T.; Snurr, R. Q.; Hupp, J. T. *Nat. Chem.* **2010**, *2*, 944–948.
(6) Bunzli, J. C. G.; Piguet, C. *Chem. Soc. Rev.* **2005**, *34*, 1048–1077.
(7) Binnemans, K. *Chem. Rev.* **2009**, *109*, 4283–4374.
(8) Cui, Y. J.; Yue, Y. F.; Qian, G. D.; Chen, B. L. *Chem. Rev.* **2012**, *112*, 1126–1162.
(9) Eliseeva, S. V.; Buenzli, J.-C. G. *Chem. Soc. Rev.* **2010**, *39*, 189–227.
(10) Callan, J. F.; Prasanna de Silva, A.; Magri, D. C. *Tetrahedron* **2005**, *36*, 8551–8588.
(11) Hu, A. G.; Ngo, H. L.; Lin, W. B. *J. Am. Chem. Soc.* **2003**, *125*, 11490–11491.
(12) Wu, C.-D.; Hu, A. G.; Zhang, L.; Lin, W. B. *J. Am. Chem. Soc.* **2005**, *127*, 8940–8941.
(13) Uemura, T.; Kitaura, R.; Ohta, Y.; Nagaoka, M.; Kitagawa, S. *Angew. Chem., Int. Ed.* **2006**, *45*, 4112–4116.
(14) Yoshizawa, M.; Tamura, M.; Fujita, M. *Science* **2006**, *312*, 251–254.
(15) Li, J. R.; Kuppler, R. J.; Zhou, H.-C. *Chem. Soc. Rev.* **2009**, *38*, 1477–1504.
(16) Bergmann, O.; Bhardwaj, R. D.; Bernard, S.; Zdunek, S.; Barnabé-Heider, F.; Walsh, S.; Zupicich, J.; Alkass, K.; Buchholz, B. A.; Druid, H.; Jovinge, S.; Frisén, J. *Science* **2009**, *324*, 98–102.
(17) Zhang, J. P.; Chen, X. M. *J. Am. Chem. Soc.* **2008**, *130*, 6010–6017.
(18) Jiao, L. Y.; Zhang, L.; Wang, X. R.; Diankov, G.; Dai, H. J. *Nature* **2009**, *458*, 877–880.
(19) Hembury, G. A.; Borovkov, V. V.; Inoue, Y. *Chem. Rev.* **2008**, *108*, 1–73.
(20) Ma, L. Q.; Abney, C.; Lin, W. B. *Chem. Soc. Rev.* **2009**, *38*, 1248–1256.
(21) Allendorf, M. D.; Bauer, C. A.; Bhakta, R. K.; Houk, R. J. T. *Chem. Soc. Rev.* **2009**, *38*, 1330–1352.
(22) McKinlay, A. C.; Morris, R. E.; Horcajada, P.; Férey, G.; Gref, R.; Couvreur, P.; Serre, C. *Angew. Chem., Int. Ed.* **2010**, *49*, 6260–6266.
(23) Liang, L.; Peng, G.; Ma, L.; Sun, L.; Deng, H.; Li, H.; Li, W. S. *Cryst. Growth Des.* **2012**, *12*, 1151–1158.
(24) Pasatoiu, T. D.; Tiseanu, C.; Madalan, A. M.; Jurca, B.; Duhayon, C.; Sutter, J. P.; Andruh, M. *Inorg. Chem.* **2011**, *50*, 5879–5889.
(25) Sarma, D.; Mahata, P.; Natarajan, S.; Panissod, P.; Rogez, G. *Inorg. Chem.* **2012**, *51*, 4495–4501.
(26) Cao, F.; Wang, S. N.; Li, D. C.; Zeng, S. Y.; Niu, M. J.; Song, Y.; Dou, J. M. *Inorg. Chem.* **2013**, *52*, 10747–10755.
(27) Huang, X. F.; Ma, J. X.; Liu, W. S. *Inorg. Chem.* **2014**, *53*, 5922–5930.
(28) Eddaoudi, M.; Moler, D. B.; Li, H. L.; Chen, B. L.; Reineke, T. M.; O'Keeffe, M.; Yaghi, O. M. *Acc. Chem. Res.* **2001**, *34*, 319–330.

(29) Tranchemontagne, D. J.; Mendoza-Cortes, J. L.; O'Keeffe, M.; Yaghi, O. M. *Chem. Soc. Rev.* **2009**, *38*, 1257−1283.
(30) Chui, S. S.-Y.; Lo, S. M.-F.; Charmant, J. P. H.; Orpen, A. G.; Williams, I. D. *Science* **1999**, *283*, 1148−1150.
(31) Ma, S.; Sun, D.; Ambrogio, M.; Fillinger, J. A.; Parkin, S.; Zhou, H.-C. *J. Am. Chem. Soc.* **2007**, *129*, 1858−1859.
(32) Furukawa, H.; Go, Y. B.; Ko, N.; Park, Y. K.; Uribe-Romo, F. J.; Kim, J.; O'Keeffe, M.; Yaghi, O. M. *Inorg. Chem.* **2011**, *50*, 9147−9152.
(33) Chen, B.; Eddaoudi, M. S.; Hyde, T.; O'Keeffe, M.; Yaghi, O. M. *Science* **2001**, *291*, 1021−1023.
(34) Zhao, D.; Timmons, D. J.; Yuan, D. Q.; Zhou, H.-C. *Acc. Chem. Res.* **2011**, *44*, 123−133.
(35) Almeida Paz, F. A.; Klinowski, J.; Vilela, S. M. F.; Tomé, J. P. C.; Cavaleiro, J. A. S.; Rocha, J. *Chem. Soc. Rev.* **2012**, *41*, 1088−1110.
(36) Weilandt, T.; Kiehne, U.; Bunzen, J.; Schnakenburg, G.; Lutzen, A. *Chem.—Eur. J.* **2010**, *26*, 2418−2426.
(37) Arouss, B. E.; Zebret, S.; Besnard, C.; Perrottet, P.; Hamacek, J. *J. Am. Chem. Soc.* **2011**, *133*, 10764−10767.
(38) Furukawa, H.; Ko, N.; Go, Y. B.; Aratani, N.; Choi, S. B.; Choi, E.; Yazaydin, A. Ö.; Snurr, R. Q.; O'Keeffe, M.; Kim, J.; Yaghi, O. M. *Science* **2010**, *329*, 424−428.
(39) Zhu, N. Y.; Tobin, G.; Schmitt, W. *Chem. Commun.* **2012**, *48*, 3638−3640.
(40) Zhao, X. L.; He, H. Y.; Dai, F. N.; Sun, D. F.; Ke, Y. X. *Inorg. Chem.* **2010**, *49*, 8650−8652.
(41) *SMART, Saint and SADABS*; Bruker AXS Inc.: Madison, Wisconsin, USA, 1998.
(42) Sheldrick, G. M. *SHELXS-97, Program for X-ray Crystal Structure Determination*; University of Gottingen: Germany, 1997;.
(43) Spek, A. L. *Implemented as the PLATON Procedure, a Multipurpose Crystallographic Tool*; Utrecht University: Utrecht, The Netherlands, 1998.
(44) Blatov, V. A.; Shevchenko, A. P.; Serezhkin, V. N. *J. Appl. Crystallogr.* **2000**, *33*, 1193−1193.
(45) Chen, H.; Ma, C. B.; Yan, D. Q.; Hu, M. Q.; Wen, H. M.; Liu, Q. T.; Chen, C. N. *Inorg. Chem.* **2011**, *50*, 10342−10352.
(46) Sanudo, E. C.; Grillo, V. A.; Knapp, M. J.; Bollinger, J. C.; Huffman, J. C.; Hendrickson, D. N.; Christou, G. *Inorg. Chem.* **2002**, *41*, 2441−2450.
(47) Ghachtouli, S. E.; Guillot, R.; Aukauloo, A.; Dorlet, P.; Anxolabehere-Mallart, E.; Costentin, C. *Inorg. Chem.* **2012**, *51*, 3603−3612.
(48) Naiya, S.; Biswas, S.; Drew, M. G. B.; Gomez-García, C. J.; Ghosh, A. *Inorg. Chem.* **2012**, *51*, 5332−5341.
(49) Stamatatos, T. C.; Luisi, B. S.; Moulton, B.; Christou, G. *Inorg. Chem.* **2008**, *47*, 1134−1144.
(50) Blatov, V. A. *Struct. Chem.* **2012**, *23*, 955−963.
(51) Liu, S. J.; Jia, J. M.; Cui, Y.; Han, S. D.; Chang, Z. *J. Solid State Chem.* **2014**, *212*, 58−63.
(52) Li, J. P.; Li, L. K.; Hou, H. W.; Fan, Y. T.; Gao, L. H. *Inorg. Chim. Acta* **2009**, *362*, 4671−4677.
(53) Eryazici, I.; Farha, O. K.; Hauser, B. G.; Yazaydın, A. O.; Sarjeant, A. A.; Nguyen, S. T.; Hupp, J. T. *Cryst. Growth Des.* **2012**, *12*, 1075−1080.
(54) Liang, J.; Wang, X. L.; Jiao, Y. Q.; Qin, C.; Shao, K. Z.; Su, Z. M.; Wu, Q. Y. *Chem. Commun.* **2013**, *49*, 8555−8557.
(55) Zhang, Z. H.; Chen, S. C.; He, M. Y.; Chen, Q.; Du, M. *Cryst. Growth Des.* **2013**, *13*, 996−1001.
(56) Zhou, J. M.; Shi, W.; Xu, N.; Cheng, P. *Inorg. Chem.* **2013**, *52*, 8082−8090.
(57) Guo, J.; Ma, J. F.; Li, J. J.; Yang, J.; Xing, S. X. *Cryst. Growth Des.* **2012**, *12*, 6074−6082.
(58) Guo, J.; Ma, J. F.; Liu, B.; Kan, W. Q.; Yang, J. *Cryst. Growth Des.* **2011**, *11*, 3609−3621.
(59) Hu, J. S.; Shang, Y. J.; Yao, X. Q.; Qin, L.; Li, Y. Z.; Guo, Z. J.; Zheng, H. G.; Xue, Z. L. *Cryst. Growth Des.* **2010**, *10*, 2676−2684.
(60) Fang, H. C.; Zhu, J. Q.; Zhou, L. J.; Jia, H. Y.; Li, S. S.; Gong, X.; Li, S. B.; Cai, Y. P.; Thallapally, P. K.; Liu, J.; Exarhos, G. J. *Cryst. Growth Des.* **2010**, *10*, 3277−3284.
(61) Rao, X. T.; Song, T.; Gao, J. K.; Cui, Y. J.; Yang, Y.; Wu, C. D.; Chen, B. L.; Qian, G. D. *J. Am. Chem. Soc.* **2013**, *135*, 15559−15564.
(62) Zang, S. Q.; Cao, L. H.; Liang, R.; Hou, H. W.; Mak, T. C. W. *Cryst. Growth Des.* **2012**, *12*, 1830−1837.
(63) Liang, X. Q.; Zhou, X. H.; Chen, C.; Xiao, H. P.; Li, Y. Z.; Zuo, J. L.; You, X. Z. *Cryst. Growth Des.* **2009**, *9*, 1041−1053.
(64) Niu, D.; Yang, J.; Guo, J.; Kan, W. Q.; Song, S. Y.; Du, P.; Ma, J. F. *Cryst. Growth Des.* **2012**, *12*, 2397−2410.
(65) Colacio, E.; Kivekäs, R.; Lloret, F.; Sunberg, M.; Suarez-Varela, J.; Bardají, M.; Laguna, A. *Inorg. Chem.* **2002**, *41*, 5141−5149.
(66) Yoo, D. H.; Cuong, T. V.; Luan, V. H.; Khoa, N. T.; Kim, E. J.; Hur, S. H.; Hahn, S. H. *J. Phys. Chem. C* **2012**, *116*, 7180−7184.
(67) Makiura, R.; Motoyama, S.; Umemura, Y.; Yamanaka, H.; Sakata, O.; Kitagawa, H. *Nat. Mater.* **2010**, *9*, 565−571.
(68) Liu, K.; You, H. P.; Zheng, Y. H.; Jia, G.; Song, Y. H.; Huang, Y. J.; Yang, M.; Jia, J. J.; Guo, N.; Zhang, H. J. *J. Mater. Chem.* **2010**, *20*, 3272−3279.
(69) Jin, X.-H.; Ren, C.-X.; Sun, J.-K.; Zhou, X.-J.; Cai, L.-X.; Zhang, J. *Chem. Commun.* **2012**, *48*, 10422−10424.
(70) Mulfort, K. L.; Farha, O. K.; Malliakas, C. D.; Kanatzidis, M. G.; Hupp, J. T. *Chem.—Eur. J.* **2010**, *16*, 276−281.
(71) Wang, R. M.; Meng, Q. G.; Zhang, L. L.; Wang, H. F.; Dai, F. N.; Guo, W. Y.; Zhao, L. M.; Sun, D. F. *Chem. Commun.* **2014**, *50*, 4911−4914.